

JGR Space Physics

RESEARCH ARTICLE

10.1029/2019JA026958

Key Points:

- The stochastic component of total electron content (TEC) is a measure of ionospheric structure
- TEC structure is very nearly unaffected by direction under weak to moderate scintillation conditions
- Ionospheric structure model parameters can be estimated directly from stochastic TEC measurements

Correspondence to:

C. Rino,
crino@bc.edu

Citation:

Rino, C., Morton, Y., Breitsch, B., & Carrano, C. (2019). Stochastic TEC structure characterization. *Journal of Geophysical Research: Space Physics*, 124. <https://doi.org/10.1029/2019JA026958>

Received 22 MAY 2019

Accepted 4 SEP 2019

Accepted article online 15 OCT 2019

Stochastic TEC Structure Characterization

Charles Rino¹, Yu Morton², Brian Breitsch², and Charles Carrano¹

¹Institute for Scientific Research, Boston College, Chestnut Hill, MA, USA, ²Institute for Scientific Research, University of Colorado Boulder, Boulder, CO, United States

Abstract The global navigation satellite systems provide high-quality total electron content (TEC) measurements that are used routinely for ionospheric diagnostics. Large-scale TEC structure is a critical input for maintaining global ionospheric models. However, residual stochastic TEC structure is typically discarded as a phase-scintillation-induced error. In this paper we show that the phase-scintillation errors are a negligibly small fraction of the stochastic TEC component for most global navigation satellite system operating conditions. With three-frequency GPS satellite measurements, two independent TEC measurements can be compared to bound the scintillation-induced errors. Data analysis and simulations show that scintillation-induced errors are a small fraction of one TEC unit as long as the lower contributing frequency *S4* index is less than 0.5. To the extent that scintillation-induced errors are negligible, spectral analysis of stochastic TEC provides a direct measure of path-integrated structure. Irregularity parameter estimation can be used to estimate power law parameters, which in turn can be interpreted with a new global ionospheric structure model. We present a summary analysis of month-long series of continuous measurements at Poker Flat, Alaska. The analysis confirms the generally accepted single power law model for high-latitude structure. A small fraction of the measurements indicate an outer-scale transition at approximately 17 km. The general pattern of the structure occurrence is consistent with auroral-zone activity.

1. Introduction

This paper will show that scintillation-induced total electron content (TEC) errors are negligible under propagation conditions that prevail for most global navigation satellite system (GNSS) observations. Anticipating this result, we first consider the interpretation of path-integrated measurements. The dynamic responses of the Earth's ionosphere to external forces and energy inputs are manifest in the electron density, $N_e(\mathbf{r}, t)$, as a function of position, \mathbf{r} , and time, t . To develop a model framework for identifying structure, we let

$$N_e(\mathbf{r}, t) = \bar{N}_e(\Delta\mathbf{r}, \Delta t) + DN_e(\Delta\mathbf{r}, \Delta t). \quad (1)$$

The coordinates $\Delta\mathbf{r}$ and Δt are confined to a region of interest (ROI) centered on a reference GPS coordinate, \mathbf{r}_0 , and evolving from a reference universal time, t_0 . The mean variation, $\bar{N}_e(\Delta\mathbf{r}, \Delta t)$, represents a deterministic component that can be characterized analytically with physics-based models.

It is well known that configurations represented by $\bar{N}_e(\Delta\mathbf{r}, \Delta t)$ may be unstable, whereby local perturbations can initiate the development of residual structure, which is represented by $DN_e(\Delta\mathbf{r}, \Delta t)$. For stochastic structure characterization, a further partitioning is introduced:

$$DN_e(\Delta\mathbf{r}, \Delta t) \simeq \Delta N_e((t - t_0) \mathbf{v}_{\text{eff}}) + \delta N_e(\Delta\mathbf{r}, \Delta t). \quad (2)$$

The term ΔN_e represents *intermediate-scale* structure that evolves slowly enough to present spatially invariant (frozen) configurations over typical measurement intervals. The term δN_e represents *small-scale* more rapidly varying spatially dispersive structure. The vector \mathbf{v}_{eff} represents the motion of the structure as measured in the ROI reference frame.

Different diagnostic measurements respond to different structure scales. For example, ionosondes measure N_e profiles with comparatively coarse resolution. Spread F is a manifestation of intermediate-scale structure, but it is not a quantitative diagnostic. Coherent backscatter radars measure the Bragg wavelength component of $\delta N_e(\Delta\mathbf{r}, \Delta t)$. Backscatter time series are processed to extract Doppler shifts induced by plasma

motion. Incoherent scatter exploits theoretical power spectral density predictions to extract electron density, composition, and ion temperature estimates. However, because TEC measurements are not sensitive to wavelength-scale structure, the $\delta N_e(\Delta \mathbf{r}, \Delta t)$ contribution will not be considered further.

TEC is formally a mapping of three-dimensional ionospheric structure onto a two-dimensional measurement plane normal to the direction of path integration:

$$TEC(\mathbf{r}_\perp, t) = \int_0^L N_e(\mathbf{r}, t) ds, \quad (3)$$

where \mathbf{r}_\perp lies in the measurement plane and L is the structured path extent. Substituting the contributing terms from (1) and (2) into (3) leads to the following TEC model:

$$TEC(\mathbf{r}_\perp, t) = \overline{TEC}(\mathbf{r}_\perp, t) + \int_0^L \Delta N_e((t - t_0) \mathbf{v}_{\text{eff}}) ds. \quad (4)$$

The stochastic component is represented by the path integral.

The TEC model represented by (4) assumes that \mathbf{v}_{eff} is constant and the captured structure is statistically uniform. GNSS orbital parameters generally support time intervals of several minutes over which the path translation is nearly invariant. However, statistical uniformity is influenced by development of the intercepted structure. Thus, measurement variations from segment to segment will reflect both statistical uncertainty and structure change. The irregularity parameter estimation procedure (IPE) introduced in section 4 uses a goodness-of-fit measure to identify uniformly structured segments.

2. TEC Measurement

Following the development in Rino et al. (2018), signal intensity, $I(t)$, phase, $\phi(t)$, and delay, $\tau(t)$, can be interpreted with the signal model

$$I(t) = C/N0(t)|h(t; f)|^2 \dots, \quad (5)$$

$$\frac{\lambda}{2\pi}\phi(t) = r(t) - cK \cdot TEC(t)/f^2 - \frac{\lambda}{2\pi}\phi^s(t) \dots, \quad (6)$$

$$c\tau(t) = r(t) + cK \cdot TEC(t)/f^2 + \frac{\lambda}{2\pi}\phi^s(t) \dots, \quad (7)$$

where $r(t)$ represents true range, f is the carrier frequency, c is the vacuum velocity of light, and $\lambda = c/f$ is the carrier wavelength. Signal delay and phase have been scaled to length units. If the TEC is measured in units of 10^{16} electrons per square meter per meter of path length, the product $cK = 40.3$. The term $C/N0$ is a standard measure of the signal-to-noise ratio after pulse compression.

The signal model defined by (5)–(7) differs from standard models only by the explicit identification of the complex modulation induced by ionospheric structure

$$h(n\Delta t, f) = |h(n\Delta t, f)| \exp\{i\phi^s(t)\}. \quad (8)$$

It is intended to capture the dominant contributions exclusive of biases, noise, and an $M\pi$ phase ambiguity that must be accommodated. The signal model is applicable for typical GNSS bandwidths and the full range of scintillation conditions typically encountered. However, identifying TEC and phase-scintillation contributions by their respective frequency dependencies is a significant departure from most phase-scintillation studies. Phase scintillation is most often extracted as a residual after detrending to remove large-scale structure. The intent is to generate a phase-scintillation realization with the same Doppler frequency content as the corresponding intensity scintillation realization. As defined here, TEC and phase have overlapping Doppler frequency content.

Standard GNSS processing operations use the absolute delay (7) to remove the $M\pi$ ambiguity. Dual-frequency measurements are then used to eliminate the $r(t)$ contribution in (6). The results are called

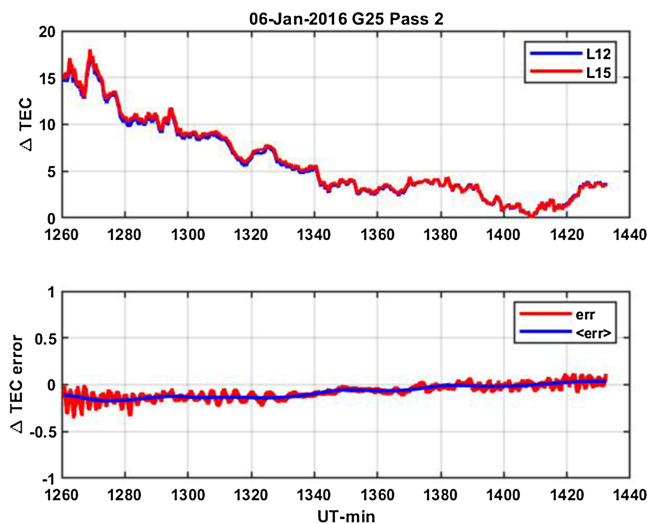


Figure 1. Upper frame shows the L12 (blue) and L15 (red) ΔTEC estimates for the representative Poker Flat pass identified in the slide title. The lower frame shows the ΔTEC error with an estimate of the mean overlaid (blue). TEC = total electron content.

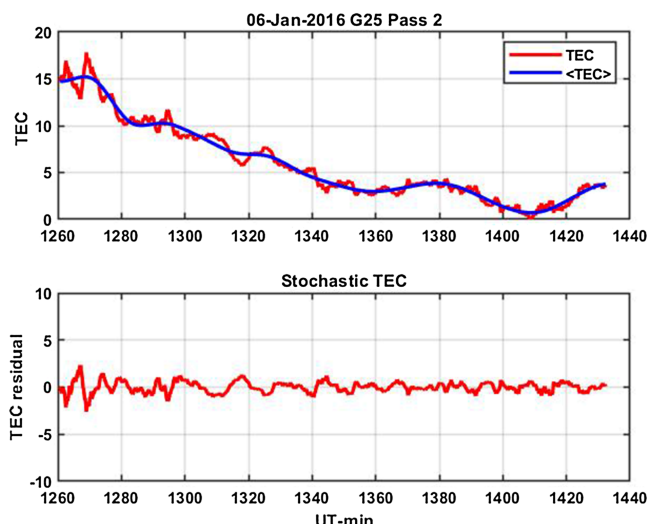


Figure 2. Upper frame shows ΔTEC defined as the average of the L12 and L15 estimates shown in the upper frame of Figure 1. The blue curve is an estimate of the TEC mean. The residual stochastic TEC is shown in the lower frame. TEC = total electron content.

geometry-free combinations. With subscripted parameters representing time samples at Δt intervals, the geometry-free combinations are scaled to ΔTEC estimates as follows:

$$\Delta TEC_n = \frac{\phi_n^{(2)}/f_2 - \phi_n^{(1)}/f_1}{2\pi K(1/f_2^2 - 1/f_1^2)} + \frac{\phi_n^{(s2)}/f_2 - \phi_n^{(s1)}/f_1}{2\pi K(1/f_2^2 - 1/f_1^2)} + \dots \quad (9)$$

The ΔTEC notation is used to indicate that the results are uncalibrated with the minimum TEC set to zero for comparisons.

As with a single phase measurement, the phase-scintillation contribution in (9) cannot be isolated. However, a subset of the GPS satellites transmit L1, L2, and L5 frequencies. The L2 and L5 frequencies are too close for definitive measurement, but the L1-L2 (L12) and L1-L5 (L15) combinations have comparable frequency separation. The difference between the L12 and L15 TEC estimates eliminates the TEC contribution to (9). If we assume that the individual errors are uncorrelated, the variance of the difference is the sum of the variances of the individual TEC estimates, which provides a bound on the scintillation-induced errors. In the following analysis, the difference between the two TEC estimates divided by two is used as a TEC error estimate.

2.1. Poker Flat Data

To explore ϕ_s -induced TEC errors, GPS data recorded at Poker Flat, Alaska, during January 2016 were made available by the University of

Colorado. The data were recorded with a Septentrio PolarRXS5 receiver, which provided phase at 100 Hz, C/NO at 50 Hz, and pseudo-range at 1 Hz. The phase data were aligned with the pseudo-range data to remove 2π ambiguities. Phase data from the 11 GPS satellites with L1, L2, and L5 signals were then processed to generate L1-L2 (L12) and L1-L5 (L15) ΔTEC_n estimates as defined by (9). Offsets were added to place the smallest ΔTEC estimate at zero for comparison.

The upper frame of Figure 1 shows representative Poker Flat L12 (blue) and L15 (red) TEC estimates. The lower frame shows the TEC error (red), which is defined as half the difference between the L12 and L15 estimates. An estimate of the mean error variation is overlaid (blue). There is a small trend, which has been associated with transmit antenna phase center offsets. With or without the bias, the TEC errors are a small fraction of one TEC unit. A wavelet-based detrending operation was used to partition the data into trend-like and residual variations. Wavelet-based detrending does not impose a rigid Doppler frequency separation.

The upper frame of Figure 2 shows the ΔTEC estimate obtained by averaging the L12 and L15 estimates shown in the upper frame of Figure 1. An estimate of the mean is overlaid in blue. The residual, stochastic TEC is shown in the lower frame. Analyzing TEC structure has been pursued by other researchers, as will be discussed in section 4. We emphasize here that the TEC estimate has very small TEC errors.

The upper frame of Figure 3 shows L1 and L2 S4 scintillation index estimates derived from 5-min data segments. The L5 S4 index is generally too close to the L2 S4 estimate to resolve. The center frame is formally the root mean square (rms) TEC rate of change over the segment, which can be identified as a rate-of-TEC change (ROTI) measure. The standard ROTI measure is usually computed with larger time steps. The lower frame shows the segment rms TEC errors for the representative example.

To show that the example selected for illustrative purposes is truly representative, Figure 4 summarizes the results from more than 25,000 January 2016 data segments. The upper frame shows probability distributions of the L1 and L2 S4 estimates. The January 2016 period was magnetically quiet, but some of the L2 estimates achieved moderate S4 values exceed-

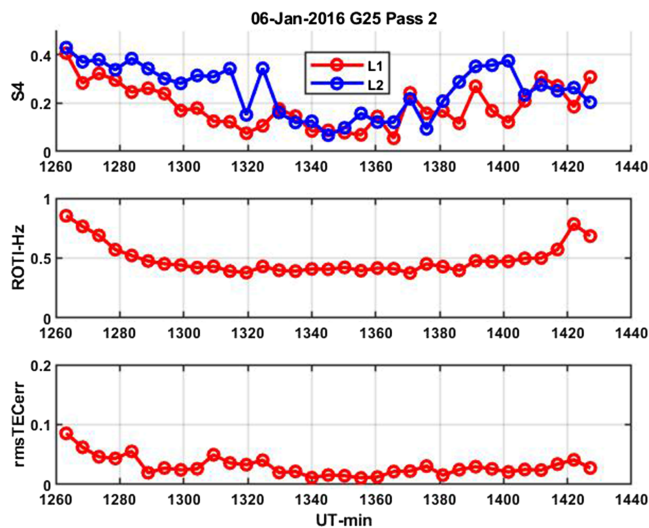


Figure 3. Upper frame shows L1 (blue) and L2 (red) S4 estimates plotted at the center of the 5-min measurement interval. Middle frame show ROTI. Lower frame show rms TEC error. TEC = total electron content; ROTI = rate-of-TEC change; rms = root mean square.

ing 0.5. The middle frame shows the probability distribution of the rms TEC errors. The S4 and TEC error distributions are similar, which indicates that higher S4 levels cause larger errors, as expected. However, over the entire weak to moderate S4 range sampled, the scintillation-induced TEC errors remain a small fraction of one TEC unit. The lower frame shows the probability distribution of the ROTI standard deviation estimates. The distribution has a second local maxima with no counterpart in the S4 distribution. Because stochastic TEC structure contains scales that map directly onto signal phase, uncorrelated ROTI and S4 variations are possible. A more detailed analysis of the relation of stochastic TEC structure and intensity scintillation will be presented in section 4.

2.2. Simulation TEC Error Analysis

Analysis of L1, L2, and L5 GPS TEC measurements showed that scintillation-induced phase errors are small for the prevailing weak to moderate scintillation conditions. Although phase scintillation defined by its departure from a $1/f_c$ frequency dependence of stochastic TEC is not directly accessible, stochastic TEC initiates phase-screen realizations of GNSS scintillation. Phase scintillation is the difference between the initiating stochastic TEC and the phase of the complex field realization. With this in mind, the multifrequency

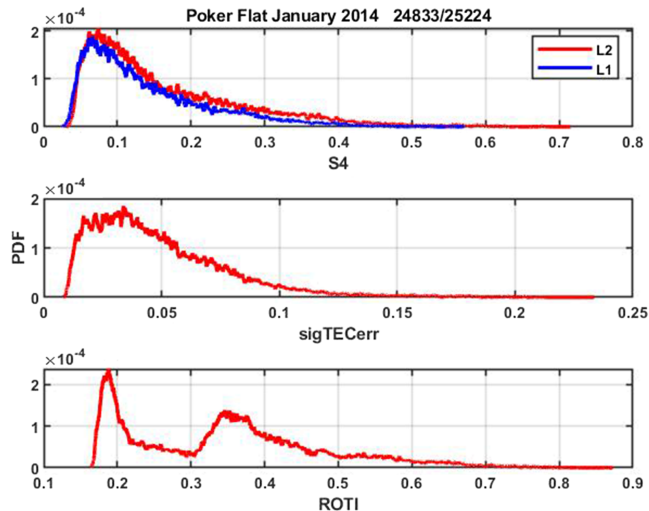


Figure 4. PDF summaries of Poker Flat intensity (upper frame), stochastic TEC (middle frame), and rate of change of TEC (lower frame). TEC = total electron content; ROTI = rate-of-TEC change; PDF = probability density function;

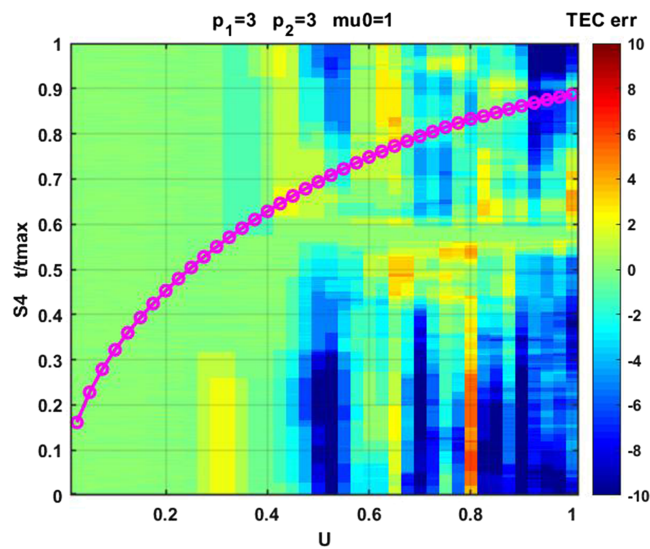


Figure 5. Display of TEC errors versus U derived from GPS multifrequency model simulations. L2 S_4 index is overlaid in magenta. The y scale is S_4 or scan distance divided by the interval length. TEC = total electron content.

GPS scintillation model described in Rino et al. (2018) has been used to generate L1, L2, and L5 complex signal realizations that can be processed to calculate L12 and L15 geometry-free TEC error estimates over an extended range of propagation disturbance levels.

The phase-screen realizations are derived from a two-component power law spectral density function (SDF) defined by the parameters C_s , p_1 , p_2 , and q_0 . As discussed in Carrano and Rino (2016), the phase-screen theory characterizes the intensity SDF in terms of a normalized spatial wave number $\mu = q\rho_F$. Time-to-space conversion via a scalar effective velocity, v_{eff} , converts Doppler frequency to spatial wave number. Scintillation intensity is measured by a universal parameter, U , such that $U < 1$ is associated with weak to moderate scintillation. Strong scatter develops as U approaches and exceeds unity. Complex scintillation time series were generated to match the Poker Flat segments and 100-Hz sampling.

Figure 5 shows a color-coded display of simulated segment TEC errors as a function of the two-dimensional propagation model parameters. The parameters were selected to generate weak to strong scintillation at the L1 GPS frequency. Both the U parameter and the Fresnel scale are frequency dependent as described in Rino et al. (2018). The L2 and L5 parameters were scaled from the L1 parameters. The L2 S_4 parameter is overlaid on the figure in magenta for reference. To accommodate the overlaid plots, the realization time extent was scaled to its maximum value (5 min). The results can be interpreted as distance from the initiating phase screen by extracting distance from ρ_F . The green regions represent errors smaller than one TEC unit, which conservatively covers the L2 S_4 range to just over 0.5 or $U < 0.2$. As the scintillation becomes more intense, there is a rapid increase in the TEC errors. Although there is some sensitivity to the selected structure parameters, the simulations are in agreement with and extend the TEC error analysis.

3. Stochastic Structure Models

GNSS identification of ionospheric structure generally proceeds from estimates of the intensity scintillation index and rms phase. However, GNSS operating frequencies were selected to minimize the effects of scintillation. Although the occurrence of severe scintillation can degrade or even disrupt GNSS processing, the occurrences of such events are rare. For TEC diagnostics, the situation is advantageous. The remainder of the paper will show that stochastic TEC can be processed to extract quantitative measures of ionospheric structure. The underlying structure models are intrinsically part of ionospheric scintillation models. This section summarizes material developed in Rino et al. (2019), which used new structure models to validate scintillation analysis procedures.

Stochastic structure models address the second term in (4), which is rewritten here as

$$\Delta \text{TEC}(\vec{\rho}) = \int_0^L \Delta N_e(x, \vec{\rho}) dx. \quad (10)$$

The vector $\vec{\rho}$ is the projection of $\mathbf{v}_{\text{eff}}\Delta t$ onto the measurement plane. We assume that $\Delta N_e(x, \vec{\rho})$ has sufficient statistical regularity to support a three-dimensional SDF, $\Phi_{\Delta N_e}(\kappa_x, \vec{\kappa})$. The measurable one-dimensional SDF from a scan along the y direction can be computed as follows:

$$\Phi_{\Delta TEC}(\kappa_y) = L \int \int \frac{\sin^2(\kappa_x L/2)}{(\kappa_x L/2)^2} \Phi_{\Delta N_e}(\kappa_x, \kappa_y, \kappa_z) \frac{d\kappa_x}{2\pi} \frac{d\kappa_z}{2\pi}. \quad (11)$$

For field-aligned propagation, we assume no variation along the x axis, whereby

$$\Phi_{\Delta N_e}(\kappa_x, \kappa_y, \kappa_z) = \Phi_{\Delta N_e}(\kappa_y, \kappa_z) 2\pi\delta(\kappa_x). \quad (12)$$

Substituting (12) into (11), it follows that

$$\Phi_{\Delta TEC}(\kappa_y) = L \int \Phi_{\Delta N_e}(\kappa_y, \kappa_z) \frac{d\kappa_z}{2\pi}, \quad (13)$$

which differs from the one-dimensional in situ SDF only by the scale factor, L . Similarly, for cross-field propagation, the κ_z variation is singular, whereby

$$\Phi_{\Delta TEC}(\kappa_y) = L \int \frac{\sin^2(\kappa_x L/2)}{(\kappa_x L/2)^2} \Phi_{\Delta N_e}(\kappa_x, \kappa_y) \frac{d\kappa_x}{2\pi}. \quad (14)$$

For cross-field path integration, the $\sin^2(\kappa_x L/2)/(\kappa_x L/2)^2$ weighting must be taken into account.

An analytic expression for $\Phi_{\Delta N_e}(\kappa_x, \vec{\kappa})$ is needed to explore the ramifications of the $\sin^2(\kappa_x L/2)/(\kappa_x L/2)^2$ weighting. The following ionospheric structure model was developed in Rino et al. (2019):

$$\Phi_{\Delta N_e}(\kappa_\tau) \simeq C_s^{(2)} \begin{cases} \kappa_\tau^{-p_1} & \text{for } \kappa_\tau \leq \kappa_0 \\ \kappa_0^{p_2-p_1} \kappa_\tau^{-p_2} & \text{for } \kappa_\tau > \kappa_0 \end{cases}. \quad (15)$$

The model characterizes the isotropic cross-field spectral density in a field-aligned ζst coordinate system, where ζ is measured along the direction of the magnetic field with st measured in the cross-field directions. In the spectral domain, $\kappa_\tau = \sqrt{\kappa_s^2 + \kappa_t^2}$. As described in Rino et al. (2019), a formal extension to three dimensions is realized with a rotation matrix that transforms the ROI coordinates κ_x , κ_y , and κ_z to the cross-field coordinates. The general relation,

$$\Phi_{\Delta N_e}(\kappa_y) = \int \Phi_{\Delta N_e}(\kappa_y, \kappa_z) \frac{d\kappa_z}{2\pi}, \quad (16)$$

defines the one-dimensional SDF, which has the similar power law form

$$\Phi_{\Delta N_e}(q) \simeq C_s^{(1)} \begin{cases} q^{-\eta_1} & \text{for } q \leq q_0 \\ q_0^{\eta_2-\eta_1} q^{-\eta_2} & \text{for } q > q_0 \end{cases}, \quad (17)$$

with $p_n = \eta_n + 1$. A scale factor provides a consistent relation between $C_s^{(1)}$ and $C_s^{(2)}$. We see that four parameters, namely, $C_s^{(2)}$, p_1 , κ_0 , and p_2 , completely define the ionospheric structure.

The defining parameters in (17) can be derived from spectral analysis of in situ data. The relation between the measured parameters and the ionospheric structure model parameters in (15) requires an evaluation of (16). However, one generally finds that $p_n \simeq \eta_n + 1$. Similarly, spectral analysis of stochastic TEC structure can use to estimate two-component power law parameters. Relating these parameters to the ionospheric structure model requires evaluation of (11). Using numerical integration to evaluate (11) with the three-dimensional SDF defined by (15), it was shown in Rino et al. (2019) that $\Phi_{\Delta TEC} \approx L\Phi_{\Delta N_e}(\kappa_y)$. In effect, the one-dimensional stochastic TEC SDF is similar to the in situ SDF. However, there are some caveats. Figure 6 in Rino et al. (2018) shows an example from simulated data. The results summarized in this section provide a framework for interpreting structure parameters derived from spectral analysis of stochastic TEC measurements.

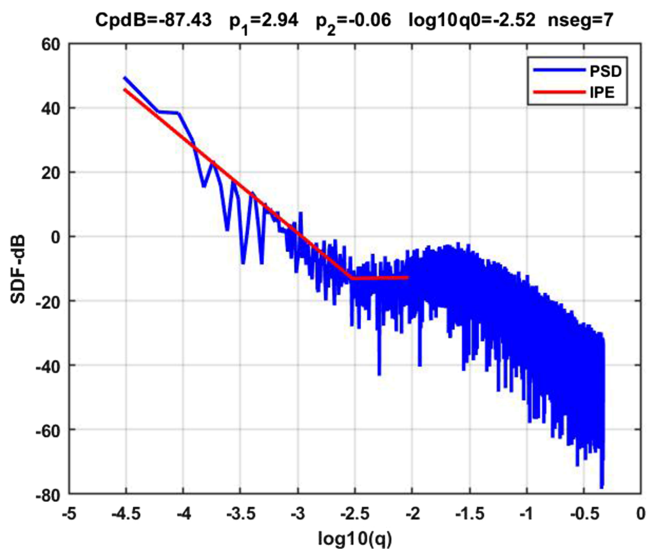


Figure 6. Example of noise contamination for weak structure levels. PSD = power spectral density; SDF = spectral density function.

4. Stochastic TEC Diagnostic Measurements

The analysis of stochastic TEC structure is not new. The simple fact that TEC structure can be measured directly, whereas phase structure, however it is identified, must be separated from the dominant range contribution suggests using TEC for structure analysis. Papers by Nickisch (2004) and van de Kamp and Cannon (2009) are exemplary. Both studies performed spectral analysis on TEC structure to determine turbulent strength and power law index parameters. The study by Nickisch was confined to high latitudes, which are directly comparable to the Poker Flat data. The van de Kamp-Cannon study included low-latitude data from Ascension Island. Both studies used least-squares fits to log-log SDF versus frequency estimates.

A more robust IPE procedure described in Rino and Carrano (2018) was used for the analysis in this paper. The maximum-likelihood procedures exploits a known exponential probability distribution of periodogram estimates relative to the mean. With the possibility that TEC and in situ one-dimensional SDFs are similar, as discussed in section 3, we use (16) as a theoretical model. With no constraints on the relative magnitudes of the estimated η_1 and η_2 parameters, we found that a significant fraction of the η_1 estimates exceed η_2 . It was found from an inspection of the SDFs that the small-scale index was capturing phase noise. Figure 6 shows an example. For summary analysis, the noise-contaminated estimates were reported as single power law SDFs.

It is also desirable to compensate for penetration-point velocity variation. A reference penetration-point altitude of 350 km was used. The propagation geometry is computed from known RINEX orbital elements. The scan distance was calculated from the translation of the penetration point. The correction for magnetic-field aspect was found to be small and was neglected. No attempt was made to estimate the drift velocity. For more refined studies, the time-to-space conversion details can be varied.

Probability distributions of the edited IPE parameters are shown in Figure 7. The η_1 - η_2 distributions show a predominantly single power law population. However, there is a small subpopulation of two-component power law segments. The lower frame shows the distribution of the break scale for these results. The most probable value after conversion to scale length (17.8 km) is shown in the figure. Two-component power law SDFs have been associated with nighttime equatorial spread *F* structure. These results show that high-latitude SDFs favor single power law SDFs with evidence of a transition or outer scale approaching 20 km.

Our most probable single power law η index of 2.5 is in agreement with the p index of 3 to 4 reported by Nickisch. The Ascension Island results reported in van de Kamp and Cannon (2009) showed somewhat shallower results, with a tendency for the larger turbulent strengths to be associated with shallower power law indices. It was shown in Rino and Carrano (2018) that correlations between turbulent strength and

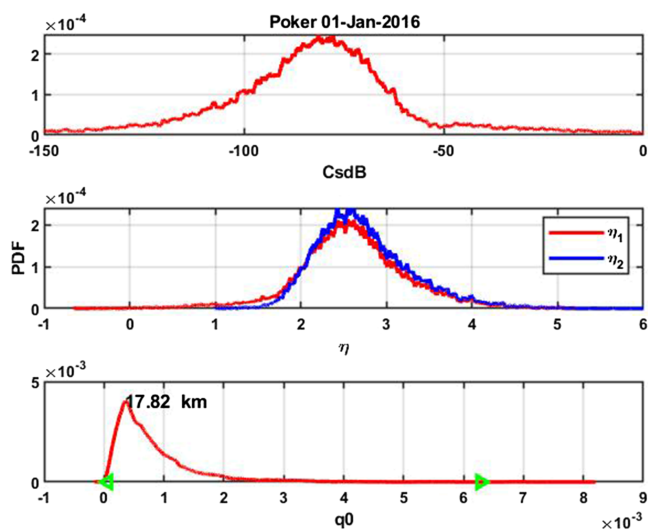


Figure 7. Probability distributions of Poker Flat irregularity parameter estimation procedure parameters. The green angle marks in the lower frame mark the intermediate scale range from 100 m to 100 km. PDF = probability density function.

large-scale power law index estimates are a direct consequence of the exponential distribution periodogram. Overall, the results reinforce our main conclusion that the signal phase structure is predominantly stochastic TEC under weak to moderate scintillation conditions.

For this study, no attempt was made to associate structure enhancements with auroral phenomena. However, to illustrate the utility of the IPE parameters for quantitative structure analysis, Figure 8 shows a color-coded display of the segment $CsdB$ estimates plotted at the 350-km path intercept point. The results provide better structure definition than the S4 or rms phase measures typically used, for example, in the extensive study by Forte et al. (2016).

5. Summary and Conclusions

The principal result in this paper was the demonstration that scintillation-induced TEC errors are negligibly small for most GNSS operating conditions. We defined phase scintillation as a residual after extraction of structure that followed the TEC $1/f_c$ frequency dependence. A phase-screen model was used to evaluate the TEC errors as a function of the propagation disturbance level. Figure 5 shows the absolute TEC error as a

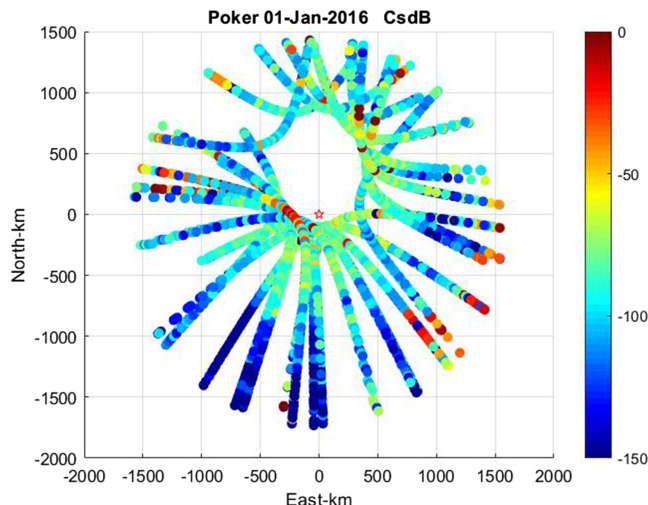


Figure 8. Geographic distribution of turbulent strength derived from high-latitude irregularity parameter estimation procedure analysis of stochastic total electron content.

function of a universal strength parameter, with the standard S_4 index as a measure. The results show that TEC errors are a fraction of one TEC unit as long as the S_4 index at the lower measurement frequency is less than 0.5.

Extracting TEC estimates from dual-frequency phase measurements was an integral part of satellite navigation long before GPS. The transit satellite very high frequency and ultrahigh frequency beacon transmissions were typically both undergoing scintillation more severe than their L-band GNSS counterparts. A study by Knepp (2004) used multiple phase-screen simulations to evaluate the transit satellite TEC scintillation error. Knepp used the term ionospheric phase to distinguish TEC from the complex signal phase in the observation plane. Knepp noted that errors were surprisingly small under weak scintillation conditions, but the errors could become very large (hundreds of radians) under strong scatter conditions.

Having established that TEC errors are negligible for weak to moderate GNSS scintillation conditions, we demonstrated an IPE procedure for extracting the defining parameters of a hypothesized two-component power law SDF. We also introduced an ionospheric structure model and reviewed the interpretation of path-integrated measures, which are common to scintillation theory. We emphasized that to the extent that stochastic TEC is a diffraction-free measure of structure, stochastic TEC is the source of the scintillation that develops as the field propagates away from the phase screen.

Finally, we note that the IPE procedure is robust and easily implemented. The IPE procedure for intensity analysis described in Carrano and Rino (2016) is more computationally demanding, although it does provide additional information. Observable systematic structure changes could provide insight into the structure mechanisms.

Acknowledgments

This work is supported by AFRL Contract FA8650-14-D-1725 17-F1033 to the University of Colorado. Poker Flat TEC data from the first two days of January 2016 are available on the Smead Aerospace Engineering Sciences Department, University of Colorado GPS laboratory website (<http://gnssrange.com/resources/data>).

References

- Carrano, C., & Rino, C. (2016). A theory of scintillation for two-component power law irregularity spectra: Overview and numerical results. *Radio Science*, 51, 789–813. <https://doi.org/10.1002/2015RS005903>
- Forte, B., Coleman, C., Skone, S., Häggström, I., Mitchell, C., Dalt, F. D., et al. (2016). Identification of scintillation signatures on GPS signals originating from plasma structures detected with EISCAT incoherent scatter radar along the same line of sight. *Journal of Geophysical Research: Space Physics*, 122, 916–931. <https://doi.org/10.1002/2016JA023271>
- Knepp, D. L. (2004). Effects of ionospheric scintillation on Transit satellite measurement of total electron content. *Radio Science*, 39, RS1S11. <https://doi.org/10.1029/2002RS002825>
- Nickisch, L. J. (2004). A power law power spectral density model of total electron content structure in the polar region. *Radio Science*, 39, RS1S12. <https://doi.org/10.1029/2002RS002818>
- Rino, C., Briestch, B., Morton, Y., Jiao, Y., Xu, D., & Carrano, C. (2018). A compact multifrequency GNSS scintillation model. *Institute of Navigation Journal*, 65, 563–569. <https://doi.org/10.1002/navi.263>
- Rino, C. L., & Carrano, C. S. (2018). On the characterization of intermediate-scale ionospheric structure. *Radio Science*, 53, 1316–1327. <https://doi.org/10.1029/2018RS006709>
- Rino, C., Carrano, C., & Groves, K. (2019). Wave propagation in extended highly anisotropic media. *Radio Science*, 54. <https://doi.org/10.1029/2019RS006793>
- Rino, C., Carrano, C., Groves, K., & Yokoyama, T. (2018). A configuration space model for intermediate-scale ionospheric structure. *Radio Science*, 53, 1472–1480. <https://doi.org/10.1029/2018RS006678>
- van de Kamp, M. M. J. L., & Cannon, P. S. (2009). Spectra of equatorial total electron content derived from gps signals. *Annales Geophysicae*, 27, 2205–2214.